

CSCPR: Cross-Source-Context Indoor RGB-D Place Recognition

Jing Liang¹, Zhuo Deng², Zheming Zhou², Min Sun², Omid Ghasemalizadeh²,
Cheng-Hao Kuo², Arnie Sen², Dinesh Manocha¹

Abstract—We present a new algorithm, Cross-Source-Context Place Recognition (CSCPR), for RGB-D indoor place recognition that integrates global retrieval and reranking into a single end-to-end model. Unlike prior approaches that primarily focus on the RGB domain, CSCPR is designed to handle the RGB-D data. We extend the Context-of-Clusters (CoCs) for handling noisy colored point clouds and introduce two novel modules for reranking: the Self-Context Cluster (SCC) and Cross Source Context Cluster (CSCC), which enhance feature representation and match query-database pairs based on local features, respectively. We also present two new datasets, ScanNetIPR and ARKitIPR. Our experiments demonstrate that CSCPR significantly outperforms state-of-the-art models on these datasets by at least 36.5% in Recall@1 at ScanNet-PR dataset and 44% in new datasets. Code and datasets will be released.

I. INTRODUCTION

Place recognition plays an important role in robotics [1], [2], [3], [4], where given query frames the goal is to identify matches from a database that share overlapping field of view with queries based on image similarities [5], [3], [4]. It is used in various applications, such as augmented reality [6], navigation [7], [4], SLAM [4], [8], etc. However, the place recognition problem is very challenging [3], [4], [2] due to: (1) different sensors, RGB, RGB-D, Lidar, etc., which require modality-specific feature processing; (2) Environmental challenges, such as illumination changes, dynamic objects, occlusion, and scale variation; (3) RGB-D indoor place recognition is not well studied [9], [4], [2], where most of the current approaches only use global retrieval for place recognition [9], [10]. Our approach focuses on the less explored domain of RGB-D indoor place recognition, and proposes an end-to-end architecture to handle both global retrieval and reranking.

RGB-D indoor place recognition is not well studied: Visual place recognition has been explored for many years, especially in RGB domain [2], [1]. However, the potential of RGB-D data is overlooked, especially for indoor environments the depth information can be crucial for place recognition [9], [10], [2]. Traditional approaches rely on global retrieval, which extracts global descriptors from each frame and ranks the database frames by the similarities with the query frame [9], [11], [12], [4]. For RGB-D place recognition, we need to handle different modalities of perceptions (color and geometry), so a good feature extractor is critical in the global retrieval. In recent years, the CoCs [13] method has been proposed and demonstrated with comparable performance with attention mechanism [14], but

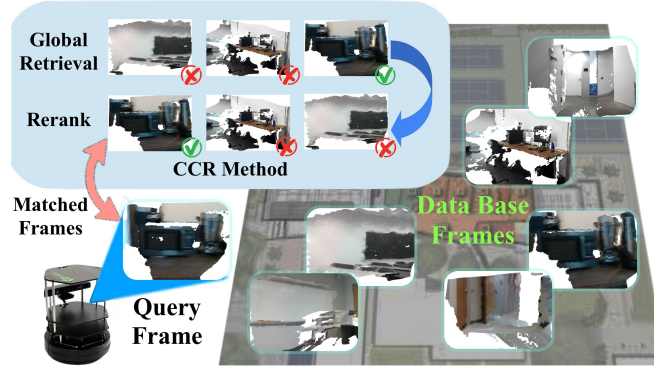


Fig. 1: **Real-world Experiment:** We propose a novel approach Cross-Source-Context Place Recognition (CSCPR) for RGB-D indoor place recognition. Given a query frame, global retrieval ranks the potentially matched frames, and our novel place-recognition reranking model reranks the candidates to achieve better recognition accuracy.

less computational cost. In our approach, CSCPR, we take advantage of the concept of CoCs, which uses higher-level global information to enhance local features and propose a novel end-to-end architecture for place recognition jointly integrating both global and local features.

RGB-D place-recognition reranking is not well studied: Reranking, as a complement to global retrieval, is to improve the accuracy by evaluating the matches of local features between the query and database frames [15], [16], [17]. Therefore, the reranking stage should be fast and accurate in matching local features. The RANSAC-based [18] methods are widely used for reranking by processing the geometric information of query-database frames [16], [17]. However, these methods only process hand-crafted geometric relations and ignores the color or other empirical features. Recently, learning-based approaches [15], [19] have been proposed that match empirical local features. However, those approaches are all for RGB-only place recognition. In this work, we generalize the learning-based reranking concept to RGB-D point cloud, and we propose a novel learning-based method for RGB-D place-recognition reranking.

The scarcity of large-scale clean dataset is a notable gap for RGB-D indoor place recognition: For indoor vision tasks, there are a bunch of datasets designed for object classification, segmentation, etc [20], [21], [22]. However, those datasets are not specifically designed for training purposes of RGB-D place recognition tasks, which require positive and negative matched frames by overlaps and large scale for training purposes [5]. HPointLoc [23] and ScanNet-PR [9]

¹ University of Maryland, College Park; ² Amazon, Bellevue, WA, USA

are recently published for RGB-D indoor place recognition tasks, but their matched pairs are selected by the distance of camera poses or point cloud distance instead of the overlap of point clouds. This makes the dataset very noisy because of some nearby point clouds with no overlaps and decreases the efficacy for training learning-based models. To bridge the gap, we introduce two large-scale clean datasets for RGB-D indoor place recognition by choosing frames with overlaps. **Main Results:** In this approach, we aim at the RGB-D indoor place recognition problem. We extend the Context Cluster concept [13] to our approach to process features. The CoCs concept enhances each local feature by the global information of the point cloud, through a cluster and dispatch mechanism. The following describes our contributions. Collectively, the contributions not only push the boundaries of RGB-D indoor place recognition to an integrated retrieval-reranking learning problem but also equip the community with data generation pipeline and new datasets for the task.

- 1) **New End-to-End Architecture for RGB-D Place Recognition:** We propose Cross-Source-Context Place Recognition (CSCPR) to integrate global retrieval and reranking. We apply the CoCs concept in these two stages to enhance the RGB-D features, especially for reranking, we propose a novel *Self-Context Cluster (SCC)*, which enhances each local feature by global information (all points features).
- 2) **Novel RGB-D Place-recognition Reranking:** For RGB-D place recognition reranking, besides the SCC model, we present a novel *Cross Source Context Cluster (CSCC)* with a simple correlation calculation to process the local matches between different point clouds for fast and accurate reranking.
- 3) **Curated Large-Scale RGB-D Indoor Place Recognition Datasets:** To address the scarcity of suitable large-scale RGB-D place-recognition datasets, we introduce ARKitIPR and ScanNetIPR RGB-D indoor place recognition task. We propose a method to generate datasets by point-cloud overlaps. The datasets contain positive and negative frames, keyframes for evaluation, poses and semantic labels of point clouds.
- 4) **Superior Performance Across Multiple Datasets:** We evaluate the performance of CSCPR on different datasets ScanNet-PR [9], ScanNetIR, and ARKitIPR. As Tab. I CSCPR achieves at least 36.5% improvement than other SOTA RGB-D indoor place recognition methods in Recall@1 in the ScanNet-PR. We also achieved at least 43.75% in ScanNetIPR and ARKitIPR. Compared with other place-recognition reranking methods, we improve at least 3.17 points in the two novel datasets. We demonstrated the effectiveness of our approach in the real-world robot.

II. RELATED WORK

Place Recognition Features and Methods: Normally, place recognition is handled by calculating the similarities/overlaps between the database and query frames. traditional methods rely on RGB image features, such as

SIFT, SURF, BoW, etc. [24], [25], [26], [27], to compose descriptors for frame matching. After convolutional networks [28] and attention mechanism [14] are proved with better performance in vision tasks, various methods [28], [29], [30] are proposed to encode frame features to global descriptors for place recognition, especially, NetVLAD-based methods [11], [12] improve performance by combining convolutions with VLAD cores for global-retrieval. The introduction of Context-of-Clusters (CoCs) [13] offers a computationally efficient yet comparably effective alternative, enhancing local features with global context. Our approach uses this concept to process and aggregate features of RGB-D point clouds.

For RGB-D indoor place recognition tasks, NetVLAD [12], ORB [31], etc. use RGB information for place recognition by comparing the global descriptors of images. MinLoc3D [32] and Point-NetVLAD [11] process point clouds, and compare point-cloud global descriptors. CGis-Net [9] applies KP-Conv [33] to encode the geometric information and enhance the features by extracting the semantic information from colors. However, these approaches typically only assess the global descriptors of RGB-D frames. We introduce a novel place-recognition reranking method to improve the accuracy of RGB-D indoor place recognition.

Place-Recognition Reranking: The accuracy of place recognition can be enhanced through a subsequent reranking stage following global retrieval [15], [16], [34]. RANSAC-based geometric verification [17], [16], [35] is a popular choice for reranking candidates. MAGSAC [36] uses a sample method NAPSAC to sample the points and apply a quality function to choose the matched pairs. PatchNetVLAD [16] uses RANSAC with scoring methods for reranking after NetVLAD [12]. Although RANSAC focuses on geometric verification, it overlooks non-geometric information. Similarly, registration tasks [37], [38], [39], [40], [41], [42] also find inliers, but those methods still attempt to match points through geometric verification or rendering without empirically learning frame similarities. Matching methods [43], [44], [45] like SuperGlue [45] identify inliers of the matching, but cannot guarantee if the frames are overlapped. Lee et al. [19] proposed CVNet-Rerank based on convolutional neural networks to process image features and compare the similarities among the features for reranking. R2Former [15] used ViTs [46] to extract the local information of images with higher attention values for reranking. However, those methods are all for RGB place recognition. RGB-D point cloud reranking still relies heavily on RANSAC-based geometric verification, Vidanapathirana et al. [17], or registration methods, Zhang et al. [34]. These approaches cannot jointly use color and geometric information effectively. We propose an end-to-end structure to jointly process RGB and geometric information and we also integrate global retrieval and reranking together for RGB-D point cloud place recognition.

III. METHOD

In this section, we first formulate the problem in Section III-A and then describe the overall architecture of CSCPR in Section III-B, which includes the Self Context Cluster (SCC) and Cross-Source Context Cluster (CSCC) modules. Finally, the training strategies are described in Section III-C.

A. Problem Definition

As with other place recognition problems [3], [4], [15], [12], the RGB-D indoor place recognition problem is defined as a point cloud retrieval problem. It's separated into two consecutive tasks, Global Retrieval [16], [11], [12], [9] and Reranking [34], [15]. In the paper, we use "frame" as an RGB-D colorized point cloud. Denote the place recognition model as M . The Global Retrieval calculates the global descriptor $\mathbf{v}_q = M(\mathbf{Q})$ of a query frame $\mathbf{Q} \in \mathcal{Q}$ and descriptor $\mathbf{v}_d = M(\mathbf{D})$ of each of the database frames $\mathbf{D} \in \mathcal{D}$. Then we compare the similarity between \mathbf{v}_q and all \mathbf{v}_d to rank the database frames. The Reranking re-estimates the similarities based on local features between \mathbf{Q} and \mathcal{D} , and generate a new ranking order. The learning objective is to ensure the similarity between the $(\mathbf{Q}, \mathbf{D}_p)$ is much bigger than the similarity between $(\mathbf{Q}, \mathbf{D}_n)$, $s(M(\mathbf{Q}), M(\mathbf{D}_p)) \gg s(M(\mathbf{Q}), M(\mathbf{D}_n))$, where $s(\cdot)$ is the similarity function and $\mathbf{D}_p \in \mathcal{D}$ and $\mathbf{D}_n \in \mathcal{D}$ correspond to the positive and negative matches from \mathcal{D} .

B. Architecture of CSCPR

The architecture of CSCPR is shown in Fig. 2. It is an end-to-end structure to jointly process the color and geometric information of the frames. It has two modules: the Global Retrieval (blue dash box) and the Reranking (yellow dash box). The inputs of CSCPR are RGB-D point clouds, $\mathcal{P} \in \mathcal{R}^{N \times 9}$, where N represents the points number and features include color $\{r, g, b\}$, 3D position $\{x, y, z\}$, and normal vector $\{n_x, n_y, n_z\}$.

The Global Retrieval model calculates the similarities between the query and database frames with their global information (global descriptors) and ranks the database frames. Thus, the critical task of this model is the feature extraction. Recently, CoCs [13] has been proposed with comparable performance to attention mechanism [14] but less computational cost. In this project, we apply CoCs structure as the backbone of the Feature Extractor and adapt it from processing RGB to point clouds by changing the reducer layers to PointConvFormer blocks [47]. We use the Farthest Point Sampling method [48] to downsample points and use the K-nearest points as the neighbors to relate the sparse and the dense points for Context Clustering [13]. In the last layer of the Feature Extractor, we aggregate the point features to global descriptors \mathbf{v}_q and \mathbf{v}_d of query and database frames by PointConvFormer. Then cosine similarity is used to measure the similarity between \mathbf{v}_d and \mathbf{v}_q . Finally, the database frames are ranked by their similarities. More details can be found in the Supplement VII-F.

The Global Retrieval model only matches the global descriptors, but some of the local information could be

missed. The Reranking model is designed to solve this issue by processing cross-source local features and estimating the similarity score between the query and database frames. There are two critical tasks for designing the Reranking model: 1. The model should be **fast** and the structure should be light in parameters and computation; 2. The structure should **effectively process the relation** of the local features from different frames. As shown in Fig. 3, to satisfy the first criterion, we design a simple structure with only three small but powerful modules. For the second criterion, we propose a novel Cross Source Context Cluster (CSCC) model to process the relation between two frames. The reranking model contains two Self Context Clusters (SCC) and one CSCC. In Fig. 2, \mathbf{f}_p^q and \mathbf{f}_p^d are the local features of the query and database frames, respectively.

Self Context Cluster (SCC) performs two functions: 1. To achieve less computational cost, it downsamples the point features to a smaller number of center features. 2. Indoor RGB-D data have large variations w.r.t perspectives, scales, and similar structures for different rooms. SCC learns features from two scales (local fine-scale feature \mathbf{f}_p with denser points from the Feature Extractors in Fig. 2 and coarse-scale feature \mathbf{f}_c with sparser centers) to tackle the challenge. To make the feature more representative, we enhance each of the center features with the global information (all point features) of the frame.

As shown in the green box of Fig. 3, inspired by attention mechanism [14], we transform the point features by projecting them into two distinct branches in SCC, reference point feature \mathbf{f}_p^r and source point feature \mathbf{f}_p^s :

$$\mathbf{f}_p^r = \|l_r(\mathbf{f}_p)\|_g \quad \text{and} \quad \mathbf{f}_c^r = \text{mean}_k(\mathbf{f}_p^r), \quad (1)$$

$$\mathbf{f}_p^s = \|l_s(\mathbf{f}_p)\|_g \quad \text{and} \quad \mathbf{f}_c^s = \text{mean}_k(\mathbf{f}_p^s), \quad (2)$$

where l_r and l_s are different Linear layers to separate the point features to reference and source features. $\|\cdot\|_g$ represents Group Norm. The geometric information of the points is used to downsample the points to a smaller number of centers by the Farthest Downsampling method, and we find the K-nearest points for each center and average the neighbors' features to a center feature \mathbf{f}_c , where \mathbf{f}_c^r and \mathbf{f}_c^s are reference and source center features.

The current center features only contain local information about the frame, and we need to enhance it with the frame's global information, which is introduced by all the point features. Thus, we compare each center feature with all point features and aggregate the most globally similar point features to the center. As in Eq. 3, the global similarity is measured by cosine distance between all \mathbf{f}_p^r and each \mathbf{f}_c^r .

$$S = \text{sig}(\alpha \cos(\mathbf{f}_c^r, \mathbf{f}_p^r) + \beta), \quad (3)$$

where α and β are trainable parameters. sig and \cos are Sigmoid and Cosine Similarity functions. $\mathbf{f}_p^r \in \mathcal{R}^{N \times D_s}$ and $\mathbf{f}_c^r \in \mathcal{R}^{M \times D_s}$, where $N > M$ are the numbers of points and centers. D_s is the feature dimension. The similarity matrix is $S \in \mathcal{R}^{M \times N}$. To reduce the computational cost, we threshold

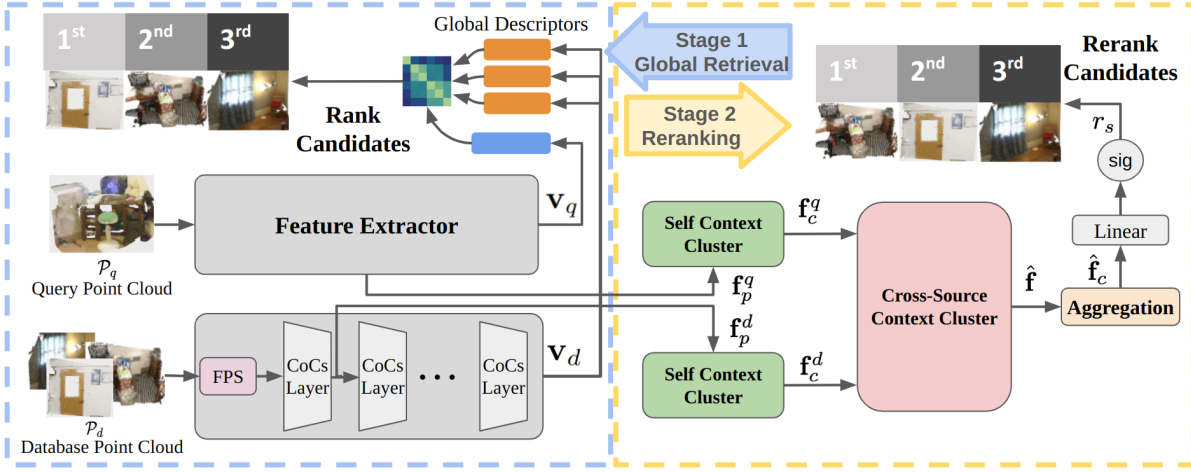


Fig. 2: **Architecture of CSCPR**: The Blue box indicates Global Retrieval, and the Yellow box represents Reranking. The global retrieval model contains a sequence of layers in the Feature Extractor. The reranking model composes Self Context Clusters (SCC) and a Cross Source Context Cluster (CSCC). After the database frames are ranked by comparing the global descriptors, \mathbf{v}_q and \mathbf{v}_d , our reranking stage calculates the relation of local features between query and database frames and aggregates the relation to reranking scores for place recognition.

the similarity matrix by only using the max similar center for each point, and setting other values as 0. To learn the representative multi-scale feature $\hat{\mathbf{f}}_c$ for reranking, according to the similarity matrix S from the reference branch, we aggregate the point features to center features in the source branch and normalize them by the similarities:

$$\tilde{\mathbf{f}}_{c,i} = \frac{1}{1 + \sum_{j=1}^N \hat{S}_{i,j}} \left(\mathbf{f}_{c,i}^s + \sum_{j=1}^N \hat{S}_{i,j} * \mathbf{f}_{p,j}^s \right) \quad (4)$$

$\mathbf{f}_{p,j}^s$ is the j_{th} vector of \mathbf{f}_p^s . $\mathbf{f}_{c,i}^s$ is the i_{th} vector of \mathbf{f}_c^s . $\hat{S} = \text{Threshold}(S)$ is the similarity matrix after threshold. The final enhanced center feature is $\hat{\mathbf{f}}_c = l_c(\tilde{\mathbf{f}}_c)$, where $l_c(\cdot)$ is a Linear layer. As demonstrated in Table III, the learned "fine-coarse" scale features $\hat{\mathbf{f}}_c$ are more effective and efficient than Attention [14], which only processes single-scale features.

Cross Source Context Cluster (CSCC) captures cross-source correlation between the query and database frames with less computational cost by processing fewer yet representative features and powerful correlation calculations. As in the red box (right side) of Fig. 3, the query and database frames have center features \mathbf{f}_c^q and \mathbf{f}_c^d , with shapes of $M_q \times D_c$ and $M_d \times D_c$, where D_c represents the feature dimension and M_q, M_d are center numbers. These sparse center features are the output of SCC, yet those features are representative in terms of multi-modality and multiple-scale information. Besides less features to compute, our correlation computation is also effective:

$$C = \text{sig}(\alpha \cos(\mathbf{f}_c^q, \mathbf{f}_c^d) + \beta), \quad (5)$$

where sig is the sigmoid function, cos is the cosine similarity function. α and β are trainable parameters. $C \in \mathcal{R}^{M_q \times M_d}$ is the Correlation matrix. We choose the top $K = 500$ center pairs according to the correlation matrix, and other correlation values are masked out as 0. Given the masked correlation, we use it as weights to concatenate

the query and retrieved candidate features together, where each concatenated feature is $\hat{\mathbf{f}}_{i,j} = l_c(C_{i,j}[\mathbf{f}_{c,i}^q, \mathbf{f}_{c,j}^d])$. l_c represents Linear layers. Therefore, weighted features from both sources empower the model to learn more effectively. Finally, the Aggregation function in Fig. 2 only aggregates the most correlated 500 features to one reranking score, r_s , as the output of CSCC:

$$\hat{\mathbf{f}}_c = \frac{1}{1 + \mathbf{c}_n} \sum_{j=1}^{M_d} \left(\frac{1}{1 + \mathbf{c}_m} \sum_{i=1}^{M_q} \hat{\mathbf{f}}_{i,j} \right), \quad (6)$$

$$\mathbf{c}_m = \sum_{i=1}^{M_q} C_{i,j}, \quad \mathbf{c}_n = \text{mean}_i \left(\sum_{j=1}^{M_d} C_{i,j} \right), \quad (7)$$

where \mathbf{c}_m is the aggregation of the correlation matrix along the dimension of query center features and \mathbf{c}_n is the aggregation of the correlation matrix along the dimension of database center features and average in the dimension of query center features. Then we have the reranking score of the database point clouds and the query point cloud: $r_s = \text{sig}(l_f(\hat{\mathbf{f}}_c))$, where l_f is a Linear layer. Bypassing the feature into a sigmoid function, we generate the reranking score r_s to rerank the candidate database frames. Our overall design is simple but effective in capturing relationships between two RGB-D clouds (see Table III).

C. Training

Training the end-to-end place recognition, CSCPR, requires multiple loss functions for Global Retrieval and Reranking. A cosine annealing scheduler [49] and Adam optimizer [50] are used to schedule the learning rates and the learning rate changes from 10^{-4} to 10^{-7} . For Global Retrieval, We use the Triplet Loss [51], \mathcal{L}_t as [52].

For Reranking, given ranked candidates, we need to refine the rank by candidates' local features, so distinguishing between query and hard negatives is crucial in this stage. Therefore, we apply hard negative mining [53] in training

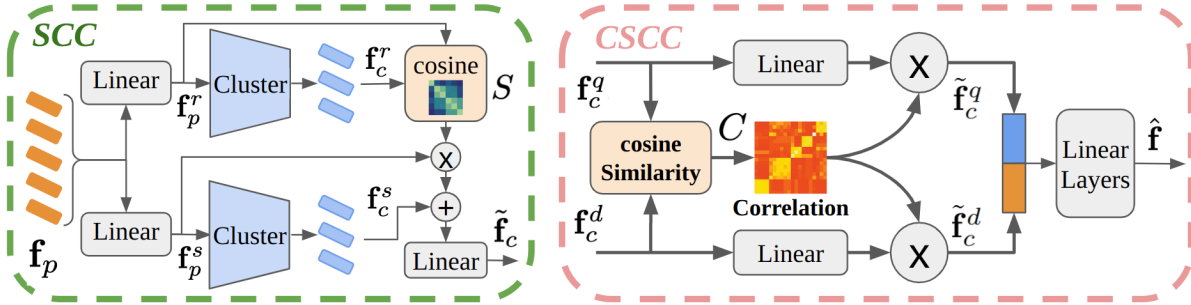


Fig. 3: **SCC and CSCC**: SCC (left) downsamples the point features f_p to center features f_c , and enhances f_c by the similarities with all f_p in the frame. CSCC calculates the correlation of the local features from these two frames and concatenates the features by the correlation relationship.

and jointly train the two stages together. Since the output similarity r_s is calculated by the Reranking model, we can use the entropy loss function

$$\mathcal{L}_c = -(y * \log(r_s) + (1 - y) * \log(1 - r_s)), \quad (8)$$

where y is the label of the matching point clouds. $y = 1$ when the point cloud matches the query point cloud, and $y = 0$ when they are not matched. The total loss function is $\mathcal{L} = \beta_t \mathcal{L}_t + \beta_c \mathcal{L}_c$, where β_t and β_c are hyperparameters, and we choose 1.0 in the training.

IV. DATASET GENERATION

Most current RGB-D indoor datasets [54], [55], [56] are designed for classification, segmentation, registration, or rendering tasks, but there are not many large-scale datasets for learning-based RGB-D indoor place recognition. ScanNet-PR [9] is designed for indoor RGB-D place recognition tasks, but because the matching frames are chosen by the distance between point clouds' centers, there is some noise in the dataset. As shown in Figure 4 in Supplement VII-A, there are cases in which point clouds are very close, but they have no overlaps. If there are no overlapping areas, the model cannot tell whether the two point clouds are in the same place. Therefore, it is also difficult to apply hard negative mining with the ScanNet-PR dataset directly, limiting the final performance of the models. To solve this issue and better evaluate the RGB-D indoor place recognition, we propose two datasets, ScanNetIPR and ARKitIPR, based on ScanNet-V2 [21] and ARKit [22]. The generated ARKitIPR dataset has 4679 scenarios and 377625 frames of point clouds in total. ScanNetIPR has 1605 scenarios and 53201 frames of point clouds in total. Both datasets contain 1. positive and negative matching frames, 2. the pose of each frame, and 3. database keyframes for the testing datasets. ScanNetIPR also provides semantic labels of the points for segmentation training. The qualitative views of the datasets are in the Supplement Section VII. Our dataset generation method can also be used in other RGB-D datasets to generate datasets for RGB-D indoor place recognition tasks.

Instead of using distance to build the dataset, because overlap of frames is the major reference for place recognition, in our approach, we use the overlap of point clouds to

determine positively or negatively matched cases. There are three steps in the data generation: 1. Choose database frames from the camera's trajectory; 2. Select positive and negative frames for each database frame among all scenarios; 3. Choose the sparse key frames for evaluation. The details of the three steps are in the Supplement VII-B

ScanNet-PR	Data Type	R@1 \uparrow	R@2 \uparrow	R@3 \uparrow
SIFT [24] + BoW [27]	RGB	16.16	21.17	24.38
NetVLAD [12]	RGB	21.77	33.81	41.49
PointNetVLAD [11]	Point Cloud	27.10	32.10	37.01
MinkLoc3D [32]	Point Cloud	15.21	19.25	22.79
Indoor DH3D [10]	RGB-D	16.10	21.92	25.30
CGiS-Net [9]	RGB-D	61.12	70.23	75.06
CGiS-Net w/o color [9]	Point Cloud	39.62	50.92	56.14
CSCPR ¹ w/o color	Point Cloud	44.24	55.11	60.18
CSCPR w/o color	Point Cloud	60.58	73.59	78.29
CSCPR ¹	RGB-D	64.63	75.02	80.09
CSCPR	RGB-D	84.14	89.82	91.25

TABLE I: **Quantitative Results**: Compared with other state-of-the-art methods, our first stage model (CSCPR¹) achieves results comparable to the best of the other methods (CGiS-Net). Our complete model with reranking improved the Recall@1 performance by at least **36.5%**.

V. EXPERIMENT

Our experimental design aims to evaluate the effectiveness and efficiency of our CSCPR against SOTA methods in RGB-D place recognition. To ensure a fair comparison, we conducted training and evaluation across both established dataset, ScanNet-PR, which uses a 3m threshold to select the database frames for place recognition, and also newly proposed datasets, ScanNetIPR and ARKitIPR, which use overlap to select frames. For each dataset, we perform both training and testing for all models. The models are trained on 8 Tesla-V100 GPUs, and the input point clouds of CSCPR are constrained to 3000 points by voxelization downsampling. Evaluations are conducted in the device with an NVIDIA RTX A5000 GPU and an Intel Xeon(R) W-2255 CPU. The primary metric used for evaluation is the Recall@k, which is the percentage of cases where at least one within top-k candidates is positive. Our experiments are structured into two distinct evaluations:

E1: End-to-End Solution Evaluation As mentioned in Section I, RGB-D indoor place recognition reranking is not well explored and we also did not find any integrated

Approaches	Data Type	Inference Time (ms)	ARKitIPR			ScanNetIPR		
			R@1 ↑	R@2 ↑	R@3 ↑	R@1 ↑	R@2 ↑	R@3 ↑
CSCPR ¹	RGB-D	-	45.04	56.20	62.24	58.10	70.33	75.95
Kabsch [57]	RGB-D	93	53.00	59.37	65.59	66.07	74.89	80.99
TEASER [58]	RGB-D	107	56.03	62.35	66.75	69.40	80.94	82.82
R2Former [15]	RGB-D	5	71.94	76.95	79.24	80.05	82.09	85.02
MAGSAC [59]	RGB	18	20.60	33.03	38.49	41.00	47.25	52.30
SuperGlue [45]	RGB	40	49.19	55.50	59.44	69.84	75.83	78.72
URR [37]	RGB-D	90	31.86	40.03	46.57	46.50	56.10	62.28
PointMBF [38]	RGB-D	300	50.12	57.30	63.47	61.27	70.92	77.40
Ours	RGB-D	4	75.13	80.24	82.33	83.22	87.76	89.30

TABLE II: **Quantitative Reranking Results:** CSCPR¹ is the global retrieval baseline. Compared with other reranking approaches, our place-recognition reranking method outperforms other approaches by at least **3.19** points in Recall@1.

Approaches	Data Type	Inference Time (ms)	ARKitIPR			ScanNetIPR		
			R@1 ↑	R@2 ↑	R@3 ↑	R@1 ↑	R@2 ↑	R@3 ↑
Attention [14]	RGB-D	11	64.14	67.65	68.81	74.95	82.94	86.22
Ours/SCC	RGB-D	3	65.56	68.39	69.11	76.52	80.03	81.03
Ours/Correlation	RGB-D	4	45.56	60.18	66.06	47.33	65.99	74.95
Ours	RGB-D	4	75.13	80.24	82.33	83.22	87.76	89.30

TABLE III: **Reranking Ablation Study:** Ours, Ours/SCC and Ours/Correlation represent our complete reranking, without SCC and without the correlation matrix, respectively. Attention represents the method with a sequence of self-cross attention blocks [14]. The table shows effectiveness of our components and the outperformance w.r.t. attention-based alternative by at least 11% in ARKitIPR and ScanNetIPR.

approaches with two stages for RGB-D place recognition. To make a fair comparison, we compare SOTA RGB-D approaches with global retrieval with our CSCPR¹ in a public large-scale RGB-D dataset, ScanNet-PR [9]. This experiment also evaluates the performance of new RGB-D point cloud-based datasets. We evaluate both RGB-D and point-cloud approaches in new datasets, ScanNetIPR and ARKitIPR.

E2: Place-Recognition Reranking Evaluation To make a fair comparison, we compare all the place-recognition reranking approaches with the same Global Retrieval stage. We evaluate the impact of our innovations, SCC and CSCC, on the reranking performance. We quantitatively and qualitatively demonstrate CSCPR’s superior reranking performance in terms of accuracy and processing speed, which are our design criteria, than various SOTA approaches.

Through this experimental design, we aim to not only validate the performance of CSCPR but also to contribute valuable datasets to the community, facilitating further advancements in RGB-D indoor place recognition.

E1 Results: In this experiment, we compare our method with SIFT [24] + BoW [60], NetVLAD [12], PointNetVLAD [11], Indoor DH3D [10], MinkLoc3D [32] and CGiS-Net [9] on public large-scale ScanNet-PR dataset. Then we demonstrate our performance on new ScanNetIPR and ARKitIPR. From Tab. IV and V in Supplement, in Recall@1, we observe our global retrieval model (CSCPR¹) has 0.5 points improvement in ScanNet-PR, 0.2 points improvement in ScanNetIPR, and around 5 points improvement in ARKitIPR because it is harder with more variety in illumination and density of the point clouds. Our integrated model, CSCPR, has at least 36.5% improvement in ScanNet-PR. We also compare our global retrieval model without color information (CSCPR¹ w/o color) with other point-cloud-based approaches and we can observe at least 4.62 improvement in Tab. I. The comparisons with novel datasets

are in Tab. I and IV in the Supplement.

E2 Results (Two sorts of comparisons): show the benefit of our learning-based place-recognition reranking:

1. Evaluate Place-Recognition Reranking Approaches: a. classical RANSAC-based geometric verification and b. learning-based place recognition reranking approaches. For a., we implement RGB-based MAGSAC [59] to fit the homography of images [16] and RGB-D-based RANSAC + Kabsch [57] and TEASER++ [58] for reranking, where Kabsch and TEASER++ calculate the transform of frames and transformed point-cloud distance is used as the geometric verification metric. For b., because of the lack of learning-based place recognition reranking works in RGB-D domain, we adapt the SOTA method, R2Former [15], from RGB domain to RGB-D point space by extending the pixel-position encoding method to $\{x, y, z\}$ positions. As shown in Tab II, we observe the learning-based approaches outperform classical approaches, where our method and R2Former outperform classical place-recognition reranking approaches by at least 28%. We observe both learning-based and classical RGB-D-based approaches outperform corresponding RGB-based approaches. CSCPR outperforms classical approaches by at least 34% and 20% at Recall@1 in ARKitIPR and ScanNetIPR. Our approach outperforms the adapted R2Former by around 3 points in both datasets at Recall@1. We observe our approach has less inference time than other approaches by at least 20%, and this satisfies our design criterion, fast and effective.

2. Evaluate Reranking-Similar Methods: a. Matching and b. registration methods are mostly used for localization [38], [58], [37], where given a pair of matched frames, the corresponding features are extracted from overlapped areas and are used to calculate transformation matrices. For a., we use RGB-based SuperGlue [45] and RGB-D-based URR [37] to calculate the matching pairs and use the number of matched pairs to determine if the frames are overlapped. For b.,

besides RANSAC-based geometric verification, we implement PointMBF [38] based on calculating the photometric error and location residual error of matched points in the query and database frames. Our method outperforms other reranking-similar approaches by at least 36% on ARKitIPR and ScanNetIPR, as shown in Tab. II.

As shown in Fig 6 in Supplement VII-D, there are two scenarios. We compare our approach, CSCPR, with the closest place-recognition reranking R2Former and TEASER++. From the bottom two rows in Figure 6, we see that R2Former can encode semantic information well where it matches the papers on the wall. However, R2Former doesn't balance geometric information effectively; while the overlapped area of the small black trash box is on the left side of the paper, it chooses the point cloud with the wrong positional relations among the door, papers, and the black box. Our approach can handle both color and geometric local information better.

E2 Results (Ablation Study): As Tab. III, we compare our approach with three different modified versions to highlight the benefits of our design. Attention [14] composes a sequence of self-attention and cross-attention models to substitute our SCC and CSCC. Our design based on the CoCs concept outperforms attention-based alternatives by at least 11% on ARKitIPR and ScanNetIPR in Recall@1 and is also faster. SCC improves the performance by at least 9% on the two datasets by enhancing the local features with global information. We also observe the correlation matrix is critical in reranking, and improves by at least 65% on two datasets, as discussed in Section III-B, which provides the relationship between two frames. These results demonstrate the effect of our innovative components (SCC and CSCC) and the efficacy of generalizing the CoCs concept to RGB-D point cloud for feature processing in RGB-D place recognition reranking.

VI. CONCLUSION, LIMITATIONS, AND FUTURE WORK

We explored the RGB-D place recognition with an integrated mechanism for both global retrieval and reranking. By developing a fast and effective reranking model, we close the gap between RGB-D place recognition reranking and learning-based algorithms. We generalized the CoCs concept to noisy colorized point cloud feature processing and demonstrated better performance in place recognition tasks. We handle the scarcity of RGB-D place recognition datasets and propose a data generation pipeline for the community to explore more datasets. We introduce two large-scale RGB-D datasets for training and testing purposes. We push forward the boundary of RGB-D indoor place recognition accuracy by demonstrating our design outperforming other SOTA approaches by at least 36.5 in Recall@1 in the ScanNet-PR dataset. For limitations, if the overlapping areas do not have many features, our method may not work well. As part of future work, we would like to apply semantic pretraining to the model to improve its understanding of the environment.

- [1] S. Garg, T. Fischer, and M. Milford, "Where is your place, visual place recognition?" in *Proceedings of the Thirtieth International Joint Conference on Artificial Intelligence, IJCAI-21*, Z.-H. Zhou, Ed. International Joint Conferences on Artificial Intelligence Organization, 8 2021, pp. 4416–4425, survey Track. [Online]. Available: <https://doi.org/10.24963/ijcai.2021/603>
- [2] S. Lowry, N. Sünderhauf, P. Newman, J. J. Leonard, D. Cox, P. Corke, and M. J. Milford, "Visual place recognition: A survey," *IEEE transactions on robotics*, vol. 32, no. 1, pp. 1–19, 2015.
- [3] Y. Liu, Y. Zhang, Y. Wang, F. Hou, J. Yuan, J. Tian, Y. Zhang, Z. Shi, J. Fan, and Z. He, "A survey of visual transformers," *IEEE Transactions on Neural Networks and Learning Systems*, 2023.
- [4] E. Yurtsever, J. Lambert, A. Carballo, and K. Takeda, "A survey of autonomous driving: Common practices and emerging technologies," *IEEE access*, vol. 8, pp. 58 443–58 469, 2020.
- [5] A. Kornilova, I. Moskalenko, T. Pushkin, F. Tojiboev, R. Tariverdizadeh, and G. Ferrer, "Dominating set database selection for visual place recognition," *arXiv preprint arXiv:2303.05123*, 2023.
- [6] S. Middelberg, T. Sattler, O. Untzelmann, and L. Kobbelt, "Scalable 6-dof localization on mobile devices," in *Computer Vision—ECCV 2014: 13th European Conference, Zurich, Switzerland, September 6–12, 2014, Proceedings, Part II 13*. Springer, 2014, pp. 268–283.
- [7] P. Mirowski, M. Grimes, M. Malinowski, K. M. Hermann, K. Anderson, D. Teplyashin, K. Simonyan, A. Zisserman, R. Hadsell *et al.*, "Learning to navigate in cities without a map," *Advances in neural information processing systems*, vol. 31, 2018.
- [8] G. Bresson, Z. Alsayed, L. Yu, and S. Glaser, "Simultaneous localization and mapping: A survey of current trends in autonomous driving," *IEEE Transactions on Intelligent Vehicles*, vol. 2, no. 3, pp. 194–220, 2017.
- [9] Y. Ming, X. Yang, G. Zhang, and A. Calway, "Cgis-net: Aggregating colour, geometry and implicit semantic features for indoor place recognition," in *2022 IEEE/RSJ International Conference on Intelligent Robots and Systems (IROS)*. IEEE, 2022, pp. 6991–6997.
- [10] J. Du, R. Wang, and D. Cremers, "Dh3d: Deep hierarchical 3d descriptors for robust large-scale 6dof relocalization," in *Computer Vision—ECCV 2020: 16th European Conference, Glasgow, UK, August 23–28, 2020, Proceedings, Part IV 16*. Springer, 2020, pp. 744–762.
- [11] M. A. Uy and G. H. Lee, "Pointnetvlad: Deep point cloud based retrieval for large-scale place recognition," in *Proceedings of the IEEE conference on computer vision and pattern recognition*, 2018, pp. 4470–4479.
- [12] R. Arandjelovic, P. Gronat, A. Torii, T. Pajdla, and J. Sivic, "Netvlad: Cnn architecture for weakly supervised place recognition," in *Proceedings of the IEEE conference on computer vision and pattern recognition*, 2016, pp. 5297–5307.
- [13] X. Ma, Y. Zhou, H. Wang, C. Qin, B. Sun, C. Liu, and Y. Fu, "Image as set of points," in *The Eleventh International Conference on Learning Representations*, 2023. [Online]. Available: <https://openreview.net/forum?id=awnvqZja69>
- [14] A. Vaswani, N. Shazeer, N. Parmar, J. Uszkoreit, L. Jones, A. N. Gomez, L. Kaiser, and I. Polosukhin, "Attention is all you need," *Advances in neural information processing systems*, vol. 30, 2017.
- [15] S. Zhu, L. Yang, C. Chen, M. Shah, X. Shen, and H. Wang, "R2former: Unified retrieval and reranking transformer for place recognition," in *Proceedings of the IEEE/CVF Conference on Computer Vision and Pattern Recognition*, 2023, pp. 19 370–19 380.
- [16] S. Hausler, S. Garg, M. Xu, M. Milford, and T. Fischer, "Patchnetvlad: Multi-scale fusion of locally-global descriptors for place recognition," in *Proceedings of the IEEE/CVF Conference on Computer Vision and Pattern Recognition*, 2021, pp. 14 141–14 152.
- [17] K. Vidanapathirana, P. Moghadam, S. Sridharan, and C. Fookes, "Spectral geometric verification: Re-ranking point cloud retrieval for metric localization," *IEEE Robotics and Automation Letters*, vol. 8, no. 5, pp. 2494–2501, 2023.
- [18] M. A. Fischler and R. C. Bolles, "Random sample consensus: a paradigm for model fitting with applications to image analysis and automated cartography," *Communications of the ACM*, vol. 24, no. 6, pp. 381–395, 1981.

- [19] S. Lee, H. Seong, S. Lee, and E. Kim, "Correlation verification for image retrieval," in *Proceedings of the IEEE/CVF Conference on Computer Vision and Pattern Recognition*, 2022, pp. 5374–5384.
- [20] C. Couprie, C. Farabet, L. Najman, and Y. LeCun, "Indoor semantic segmentation using depth information," *arXiv: Computer Vision and Pattern Recognition*, 2013. [Online]. Available: <https://api.semanticscholar.org/CorpusID:6681692>
- [21] A. Dai, A. X. Chang, M. Savva, M. Halber, T. Funkhouser, and M. Nießner, "ScanNet: Richly-annotated 3d reconstructions of indoor scenes," in *Proc. Computer Vision and Pattern Recognition (CVPR)*, IEEE, 2017.
- [22] G. Baruch, Z. Chen, A. Dehghan, T. Dimry, Y. Feigin, P. Fu, T. Gebauer, B. Joffe, D. Kurz, A. Schwartz, and E. Shulman, "ARKitscenes - a diverse real-world dataset for 3d indoor scene understanding using mobile RGB-d data," in *Thirty-fifth Conference on Neural Information Processing Systems Datasets and Benchmarks Track (Round 1)*, 2021. [Online]. Available: https://openreview.net/forum?id=tjZjv.qh_CE
- [23] D. Yudin, Y. Solomentsev, R. Musaev, A. Staroverov, and A. I. Panov, "Hpointloc: Point-based indoor place recognition using synthetic rgb-d images," in *International Conference on Neural Information Processing*. Springer, 2022, pp. 471–484.
- [24] L. David, "Distinctive image features from scale-invariant keypoints," *International journal of computer vision*, vol. 60, pp. 91–110, 2004.
- [25] M. Cummins and P. Newman, "Fab-map: Probabilistic localization and mapping in the space of appearance," *The International journal of robotics research*, vol. 27, no. 6, pp. 647–665, 2008.
- [26] D. Gálvez-López and J. D. Tardos, "Bags of binary words for fast place recognition in image sequences," *IEEE Transactions on Robotics*, vol. 28, no. 5, pp. 1188–1197, 2012.
- [27] J. Sivic and A. Zisserman, "Efficient visual search of videos cast as text retrieval," *IEEE transactions on pattern analysis and machine intelligence*, vol. 31, no. 4, pp. 591–606, 2008.
- [28] A. Gordo, J. Almazan, J. Revaud, and D. Larlus, "End-to-end learning of deep visual representations for image retrieval," *International Journal of Computer Vision*, vol. 124, no. 2, pp. 237–254, 2017.
- [29] G. Berton, R. Mereu, G. Trivigno, C. Masone, G. Csurka, T. Sattler, and B. Caputo, "Deep visual geo-localization benchmark," in *Proceedings of the IEEE/CVF Conference on Computer Vision and Pattern Recognition*, 2022, pp. 5396–5407.
- [30] H. Touvron, M. Cord, M. Douze, F. Massa, A. Sablayrolles, and H. Jégou, "Training data-efficient image transformers & distillation through attention," in *International conference on machine learning*. PMLR, 2021, pp. 10347–10357.
- [31] R. Mur-Artal and J. D. Tardós, "Orb-slam2: An open-source slam system for monocular, stereo, and rgb-d cameras," *IEEE transactions on robotics*, vol. 33, no. 5, pp. 1255–1262, 2017.
- [32] J. Komorowski, "Minkloc3d: Point cloud based large-scale place recognition," in *Proceedings of the IEEE/CVF Winter Conference on Applications of Computer Vision*, 2021, pp. 1790–1799.
- [33] H. Thomas, C. R. Qi, J.-E. Deschaud, B. Marcotegui, F. Goulette, and L. J. Guibas, "Kpconv: Flexible and deformable convolution for point clouds," in *Proceedings of the IEEE/CVF international conference on computer vision*, 2019, pp. 6411–6420.
- [34] W. Zhang, H. Zhou, Z. Dong, Q. Yan, and C. Xiao, "Rank-pointretrieval: Reranking point cloud retrieval via a visually consistent registration evaluation," *IEEE Transactions on Visualization and Computer Graphics*, 2022.
- [35] R. Wang, Y. Shen, W. Zuo, S. Zhou, and N. Zheng, "Transvpr: Transformer-based place recognition with multi-level attention aggregation," in *Proceedings of the IEEE/CVF Conference on Computer Vision and Pattern Recognition*, 2022, pp. 13648–13657.
- [36] D. Barath, J. Noskova, M. Ivashechkin, and J. Matas, "Magsac++, a fast, reliable and accurate robust estimator," in *Proceedings of the IEEE/CVF Conference on Computer Vision and Pattern Recognition (CVPR)*, June 2020.
- [37] B. et al., "Unsuperviseddr&r: Unsupervised point cloud registration via differentiable rendering," 2021.
- [38] M. Yuan, K. Fu, Z. Li, Y. Meng, and M. Wang, "Pointmbf: A multi-scale bidirectional fusion network for unsupervised rgb-d point cloud registration," in *2023 IEEE/CVF International Conference on Computer Vision (ICCV)*. Los Alamitos, CA, USA: IEEE Computer Society, oct 2023, pp. 17648–17659. [Online]. Available: <https://doi.ieeecomputersociety.org/10.1109/ICCV51070.2023.01622>
- [39] G. Mei, H. Tang, X. Huang, W. Wang, J. Liu, J. Zhang, L. Van Gool, and Q. Wu, "Unsupervised deep probabilistic approach for partial point cloud registration," in *Proceedings of the IEEE/CVF Conference on Computer Vision and Pattern Recognition*, 2023, pp. 13611–13620.
- [40] H. Jiang, Z. Dang, Z. Wei, J. Xie, J. Yang, and M. Salzmann, "Robust outlier rejection for 3d registration with variational bayes," in *Proceedings of the IEEE/CVF Conference on Computer Vision and Pattern Recognition*, 2023, pp. 1148–1157.
- [41] X. Zhang, J. Yang, S. Zhang, and Y. Zhang, "3d registration with maximal cliques," in *Proceedings of the IEEE/CVF Conference on Computer Vision and Pattern Recognition*, 2023, pp. 17745–17754.
- [42] A. Hatem, Y. Qian, and Y. Wang, "Point-tta: Test-time adaptation for point cloud registration using multitask meta-auxiliary learning," in *Proceedings of the IEEE/CVF International Conference on Computer Vision*, 2023, pp. 16494–16504.
- [43] V. Panek, Z. Kukulova, and T. Sattler, "Meshloc: Mesh-based visual localization," in *European Conference on Computer Vision*. Springer, 2022, pp. 589–609.
- [44] M. Li, Z. Qin, Z. Gao, R. Yi, C. Zhu, Y. Guo, and K. Xu, "2d3d-matr: 2d-3d matching transformer for detection-free registration between images and point clouds," in *Proceedings of the IEEE/CVF International Conference on Computer Vision*, 2023, pp. 14128–14138.
- [45] P.-E. Sarlin, D. DeTone, T. Malisiewicz, and A. Rabinovich, "Superglue: Learning feature matching with graph neural networks," in *Proceedings of the IEEE/CVF conference on computer vision and pattern recognition*, 2020, pp. 4938–4947.
- [46] A. Dosovitskiy, L. Beyer, A. Kolesnikov, D. Weissenborn, X. Zhai, T. Unterthiner, M. Dehghani, M. Minderer, G. Heigold, S. Gelly *et al.*, "An image is worth 16x16 words: Transformers for image recognition at scale," *arXiv preprint arXiv:2010.11929*, 2020.
- [47] W. Wu, L. Fuxin, and Q. Shan, "Pointconvformer: Revenge of the point-based convolution," 2023. [Online]. Available: https://openreview.net/forum?id=9jW_Oynp0au
- [48] Y. Eldar, M. Lindenbaum, M. Porat, and Y. Y. Zeevi, "The farthest point strategy for progressive image sampling," *IEEE Transactions on Image Processing*, vol. 6, no. 9, pp. 1305–1315, 1997.
- [49] I. Loshchilov and F. Hutter, "Sgdr: Stochastic gradient descent with warm restarts," *arXiv preprint arXiv:1608.03983*, 2016.
- [50] D. P. Kingma and J. Ba, "Adam: A method for stochastic optimization," *arXiv preprint arXiv:1412.6980*, 2014.
- [51] F. Schroff, D. Kalenichenko, and J. Philbin, "Facenet: A unified embedding for face recognition and clustering," in *Proceedings of the IEEE conference on computer vision and pattern recognition*, 2015, pp. 815–823.
- [52] J. Liang, Z. Deng, Z. Zhou, O. Ghasemalazadeh, D. Manocha, M. Sun, C.-H. Kuo, and A. Sen, "Poco: Point context cluster for rgb-d indoor place recognition," *arXiv preprint arXiv:2404.02885*, 2024.
- [53] J. Robinson, C.-Y. Chuang, S. Sra, and S. Jegelka, "Contrastive learning with hard negative samples," *arXiv preprint arXiv:2010.04592*, 2020.
- [54] J. Sturm, N. Engelhard, F. Endres, W. Burgard, and D. Cremers, "A benchmark for the evaluation of rgb-d slam systems," in *Proc. of the International Conference on Intelligent Robot Systems (IROS)*, Oct. 2012.
- [55] B. Glocker, S. Izadi, J. Shotton, and A. Criminisi, "Real-time rgb-d camera relocalization," in *2013 IEEE International Symposium on Mixed and Augmented Reality (ISMAR)*. IEEE, 2013, pp. 173–179.
- [56] A. Handa, T. Whelan, J. McDonald, and A. J. Davison, "A benchmark for rgb-d visual odometry, 3d reconstruction and slam," in *2014 IEEE international conference on Robotics and automation (ICRA)*. IEEE, 2014, pp. 1524–1531.
- [57] K. S. Arun, T. S. Huang, and S. D. Blostein, "Least-squares fitting of two 3-d point sets," *IEEE Transactions on pattern analysis and machine intelligence*, no. 5, pp. 698–700, 1987.
- [58] H. Yang, J. Shi, and L. Carlone, "Teaser: Fast and certifiable point cloud registration," *IEEE Transactions on Robotics*, vol. 37, no. 2, pp. 314–333, 2020.
- [59] D. Barath, J. Noskova, M. Ivashechkin, and J. Matas, "Magsac++, a fast, reliable and accurate robust estimator," in *Proceedings of the IEEE/CVF conference on computer vision and pattern recognition*, 2020, pp. 1304–1312.
- [60] E. Rublee, V. Rabaud, K. Konolige, and G. Bradski, "Orb: An efficient alternative to sift or surf," in *2011 International conference on computer vision*. Ieee, 2011, pp. 2564–2571.

VII. SUPPLEMENT

A. Dataset Differences

The dataset differences are shown in Fig. 4

B. Generating Different Datasets

The algorithm generating training data is as Algorithm 1. We use overlap to select the frames for training and evaluation with the following three steps:

The first step is to generate frames according to the motion of the camera. In contrast to the odometry tasks, place recognition does not require lots of very similar point clouds to estimate the transformation matrices, because those point clouds do not provide much different information for place retrieval and add burdens for training. Therefore, the frames are chosen by some overlap threshold along the trajectory of the camera motion, where if the current frame overlaps too much with the last frame it will be dropped, as shown in Algorithm 1. The overlap in this step is calculated by the symmetric intersection of the union (IoU) of the voxelized point clouds:

$$[\mathbf{v}_n, \mathbf{v}_l] = \text{voxelize}([p_n \mathbf{P}_n, p_l \mathbf{P}_l]), \quad (9)$$

$$\text{FrameOverlap}(\mathbf{P}_n, \mathbf{P}_l) = \frac{|v_n \cap v_l|}{|v_n \cup v_l|} \quad (10)$$

\mathbf{P}_n and \mathbf{P}_l are points chosen by frustums in the integrated point cloud of the scenario. \mathbf{v}_n and \mathbf{v}_l are the voxels of the n_{th} frame and the last selected frame, respectively. $p_n \mathbf{P}_n$ represents the point cloud transformed in the global frame. The threshold $T_c = 0.5$ is used in the data generation task.

The second step is to choose the positive frames in the same scenario and negative cases in all scenarios. Since this step treats each frame as a query frame to calculate the overlap with other frames in the scenario, the overlap is mostly w.r.t. the query frame. Therefore, an asymmetric overlap metric can be used

$$\text{Overlap}(\mathbf{P}_q, \mathbf{P}_d) = \frac{|v_q \cap v_o|}{|v_q|}, \quad (11)$$

$$\mathbf{v}_q = \text{voxelize}(\mathbf{P}_q), \quad \mathbf{v}_d = \text{voxelize}(\mathbf{P}_d) \quad (12)$$

where \mathbf{P}_q and \mathbf{P}_d are query and database point clouds. \mathbf{v}_q and \mathbf{v}_d are the voxels of these two point clouds. Then the positive frames are selected by the threshold $\text{Overlap} > T_p$. Negative frames can be selected by $\text{Overlap} \leq T_n$. Normally, the negative threshold $T_n = 0$.

The third step is to extract the key frames of each scenario, where we build a graph for each scenario using the positively matched frames and choose the dominating nodes as the keyframes of the scenario as [5], according to the connection of the graph.

The datasets are separated into training, evaluation, and testing scenarios, and each testing scenario contains database key-frames for recall calculation. ScanNetIPR contains 1605 scenarios and 53201 frames in total. For each frame, there are positively and negatively matched frames in the same scenarios. Each frame of the point cloud contains positional information x, y, z , normal information n_x, n_y, n_z , color

Algorithm 1 The frames are chosen by the motion of the camera, where we use an overlap threshold to select the representative frames for place recognition tasks. The FrameOverlap() function is as Eq. 10.

Require: N consecutive frames,

Require: $F_l \leftarrow \{\mathbf{P}_0, p_0\}$

Require: database = $\{F_l, \}$

while $n < N$ **do**

$F_n \leftarrow \{\mathbf{P}_n, p_n\}$

if $\text{FrameOverlap}(F_l, F_n) < T_c$ **then**

database.add(F_n)

$F_l = F_n$

end if

end while

information r, g, b , and also semantic labels of each point. ARKitIPR contains 4679 scenarios and 377625 frames in total. Each point cloud has positional, normal, and color information.

As shown in Figure 5, the top row contains two point clouds in a scene of ScanNetIPR and the bottom row contains two point clouds in a scene of ARKitIPR. The Normals in the figure represent the normal vectors of the points, which are shown as RGB images with the $\{n_x, n_y, n_z\}$ as $\{r, g, b\}$. The RGB-D point clouds are extracted as mentioned in Section IV. The Semantic column in ScanNetIPR is points segmentation and in ARKit is the object classification with bounding boxes.

C. Comparisons of Global Retrieval in Novel Datasets

For the evaluation of different novel datasets, from the comparison of Tab. I and IV, we observe approaches in our ScanNetIPR have lower recall values than the ScanNet-PR dataset. For evaluation using a 3-meter threshold used by ScanNet-PR results in pairs with larger overlaps on average compared to ScanNetIPR, which directly uses an overlapping threshold. Consequently, ScanNetIPR presents a greater challenge than the ScanNet-PR dataset because it includes pairs with smaller overlapping areas.

D. Qualitative Results

E. RGB-D Indoor Place Recognition Results

<i>ScanNetIPR</i>	Data Type	R@1 \uparrow	R@2 \uparrow	R@3 \uparrow
PointNetVLAD	Point Cloud	22.43	30.81	36.58
MinkLoc3D	Point Cloud	10.13	16.63	20.80
CGiS-Net	RGB-D	57.89	69.95	75.51
CSCPR ¹ w/o c	RGB-D	40.74	51.81	57.97
CSCPR w/o c	RGB-D	57.35	69.22	73.61
CSCPR ¹	RGB-D	58.10	70.33	75.95
CSCPR	RGB-D	83.22	87.76	89.30

TABLE IV: **Comparisons in New ScanNetIPR:** The ScanNetIPR is harder than ScanNetPR, where methods have relatively smaller Recall@1. Our method still outperforms other approaches for both RGB-D and pure point-cloud place recognition.

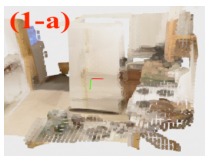
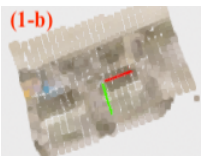




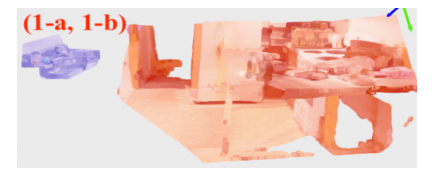


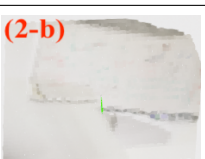
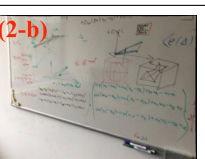
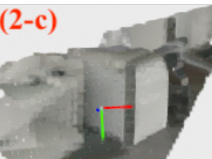




Query Frames	FPF in ScanNetPR		FPF in ScanNetIPR (Ours)	
	Points	RGB	Points	RGB
(1-a) 	(1-b) 	(1-b) 	(1-c) 	(1-c) 
(1-a) 	(1-a, 1-b) 		(1-a, 1-c) 	
(2-a) 	(2-b) 	(2-b) 	(2-c) 	(2-c) 
(2-a) 	(2-a, 2-b) 		(2-a, 2-c) 	

Fig. 4: **Furthest Positive Frame (FPF) of ScanNetPR vs. ScanNetIPR (ours)**: FPF depicts the least overlapping matched frame to the query in both datasets. For the red letters: $\{1, 2\}$ represent two cases and $\{a, b, c\}$ are query, ScanNetPR, and ScanNetIPR frames, respectively. In the first column, the 1st and 3rd rows show point clouds and the 2nd and 4th rows show the corresponding RGB images for a clearer view. In later columns, the 2nd and 4th rows show the query (red) and FPF (blue) frames in the global coordinate and their overlapped areas (green circles). In the ScanNetPR dataset, using center distance as the criterion to determine matched frames leads to erroneous classification. In ScanNetIPR, the overlap is the only criterion for matching, thus it is more accurate for training and evaluating place recognition tasks.



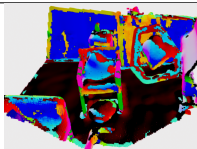



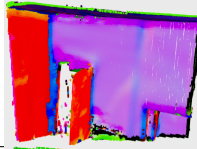

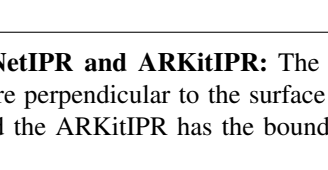



Scenes	RGB-D Points	Normals	Semantic
			
			
			

Fig. 5: **ScanNetIPR and ARKitIPR**: The top two rows show one scene of ScanNetIPR, where the normals are normal vectors that are perpendicular to the surface of the points. In ScanNetIPR, the semantic information is the segmentation of the points and the ARKitIPR has the bounding boxes.

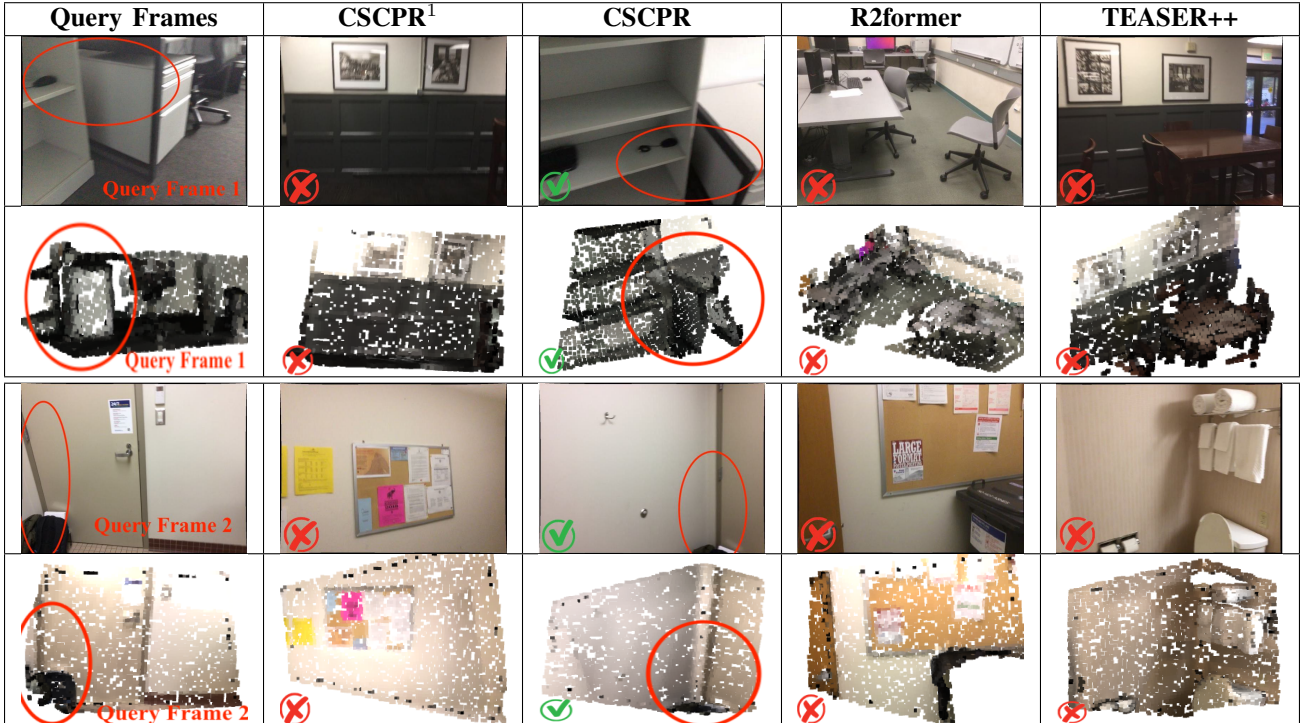


Fig. 6: **Qualitative Comparisons:** 1st and 3rd row show RGB images correspond to point clouds in 2nd and 4th rows. The red circles mark the overlapping areas between query frames (1st column) and later Recall@1 frames from different approaches. CSCPR¹ is the first stage of our method. R2Former performs closest to our approach, but its performance depends considerably on the semantic information. Our overall algorithm (CSCPR) balances the geometric and RGB information well and achieves the best performance, even for the scenarios that have very small overlapping areas.

<i>ARKitIPR</i>	Data Type	R@1 \uparrow	R@2 \uparrow	R@3 \uparrow
PointNetVLAD	Point Cloud	11.04	16.57	20.57
MinkLoc3D	Point Cloud	8.14	10.95	13.79
CGIS-Net	RGB-D	39.80	49.30	55.64
CSCPR ¹	RGB-D	45.04	56.20	62.24
CSCPR	RGB-D	75.13	80.24	82.33

TABLE V: **Comparisons in new ARKitIPR:** Our method still outperforms other approaches for both RGB-D and pure point-cloud place recognition.

F. Architecture Details

As shown in Fig 2, the global retrieval block contains four adapted CoCs layers. Each CoCs layer contains 2X PointConvFormer [47] (PCF) and 4X Context Cluster Block (CCB). Their feature dimensions are 64, 128, 320, 512, respectively. PCF and CCB in the same CoCs layer share the same feature dimension. After the 4 layers, one more PCF is used to aggregate output point features into one global descriptor with the feature dimension 512. PCF learns multi-modality feature aggregation, by enhancing the color features with the relative geometric information [47], based on KNN neighbors with sizes 98, 50, 20, 10. The points are downsampled to 800, 300, 100, 40, respectively, by FPS in the four layers. CCB performs multi-scale feature processing by enhancing the current-level point features with high-level center features. We have 300, 100, 40, 20 centers in the

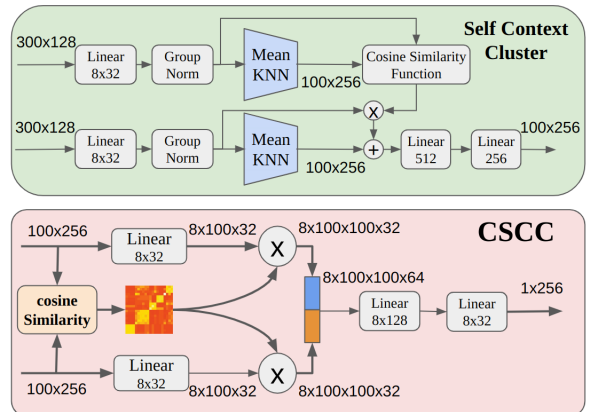


Fig. 7: **Architecture Details:** The details of the architecture of SCC and CSCC

four layers, which are down-sampled by FPS from point features. The point-to-center relation is initialized by KNN with neighbor sizes, 50, 20, 10, 10, respectively, and learned by the neural networks.

SCC and CSCC models are in Figure 7. The input of the point features from the global retrieval has the shape of 300×128 , which has 300 points. Then the points are clustered into 100 centers with the dimension of 256. Finally, the centers are processed by the correlations between the

two clouds of centers and then aggregated into a reranking score.